Physical Modelling in Geotechnics

Seismic response of an offshore wind turbine jacket structure with pile foundations

K. Natarajan & G.S.P. Madabhushi
Department of Engineering, University of Cambridge

ABSTRACT: The dynamic response of the jacket structure supporting an offshore wind turbine depends both on the axial and lateral stiffnesses of the pile foundations. Often these responses are the governing criteria for structural design. Hence, it is necessary to understand the jacket structure and foundation response under the combined action of extreme cyclic loads (wave +wind) with the dynamic (seismic) loads. Typically, the jacket structure is not susceptible to moderate level seismic acceleration, but the influence of the tower mass can excite the jacket structure and its piles. This seismic excitation causes the soil to behave nonlinearly. The nonlinear soil combined with extreme loads may lead to the settlement and rotation of the structure. A jacket-equivalent wind tower model was developed and tested with piles passing through a two-layered sandy soil. The dynamic centrifuge testing was conducted to obtain the structure's dynamic response and capture the soil behaviour. Accordingly, two centrifuge tests were conducted, the first test with dry sand and the other with saturated soil conditions. The natural frequency of the tower-jacket-soil system was determined in-flight using a sine-sweep input motion. The dynamic response of the model jacket structure was determined under strong, realistic and sinusoidal earthquakes. The key findings are that the generation of excess pore pressures causes the soil to liquefy under strong seismic acceleration, eventually leading the structure to settle and rotate more than its allowable serviceable limit states (SLS).

Keywords: jacket, earthquake, centrifuge, stiffness, pore pressure, settlement.

1 INTRODUCTION

The world is under pressure to reduce carbon emissions to net-zero, and with Glasgow Climate Pact (COP21) deals to reduce coal power, more countries are focussing on renewable energy. Power from wind energy tops the list, with offshore wind energy being the most viable resource. In order to increase power production, high capacity wind turbines become essential. Advance technological improvements made this possible with manufacturers reaching turbine capacity of 15MW to 25MW. Monopiles have dominated the world in the offshore renewable sector for more than a decade because of the smaller turbine capacity and cost-effective installation. However, with increased turbine capacity to such an enormous scale, monopile needs to be designed with larger pile diameters ranging from 8 to 15m in diameter. This increases the transportation risks as well as fabrication and installation costs.

Moreover, design aspects include *D/t* ratio limitations, fatigue problems, pile driving issues, dynamic sensitivity, and sea bed liquefaction in seismically active areas are the main constraints for monopile. Thus open up jacket structures as the best alternate option for offshore wind turbine support structures. (Hao et al., 2013) tested both monopile and three-legged jacket structure in the centrifuge and concluded that jacket structures are the better solution for mitigating lateral rotation under seismic loading and exhibits good resistance to seismic-induced settlement

Most of the offshore project sites in the Southeast Asian region are susceptible to high-intensity earthquakes, with sand layers covering the depth of 5 to 10m below the sea bed. Therefore, jackets installed in these regions require careful design consideration for soil liquefaction under seismic accelerations. Also, wind harvesters planning to install jackets in these regions require a complete understanding of the soil-structure interactions. This paper outlines the modelling and design aspect of the wind turbine jacket structure in the centrifuge scale. In addition, it compares the effects of the dry sand model with the saturated condition.

2 JACKET FOUNDATION

Several options are available to install jacket supported offshore wind farm structures. For prepiled jackets, the piles are installed first with the help of a pile template and then installing the jacket with the grouted connection between them and finally, the wind tower installation (Fig.1). In the post pile method, the jacket is installed first on the sea bed and stabilized using

© 2022 KOREAN GEOTECHNICAL SOCIETY (KGS), Seoul, Korea, ISBN 978-89-952197-7-5

mudmats and then installing the piles. In this method, the piles can be installed through the main jacket leg (Fig.2) or through the skirt legs (Fig.3). The entire jacket will act as a template for the piles in either of these options. Other option includes the suction piles wherein large diameter piles are attached to the jacket legs and installed as a single unit. Of all these options, prepiled jacket structures are the most prefered, cost-effective and proven substructures for offshore wind turbines compared to other options.

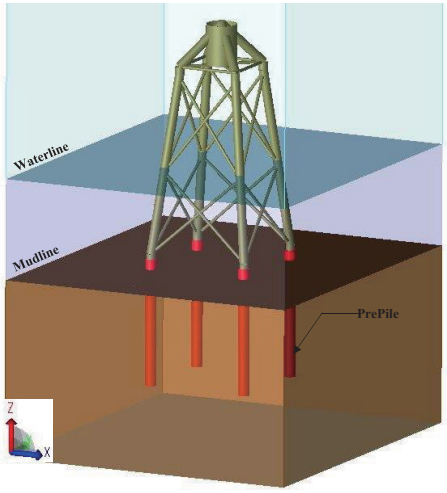

Fig. 1. Prepile option

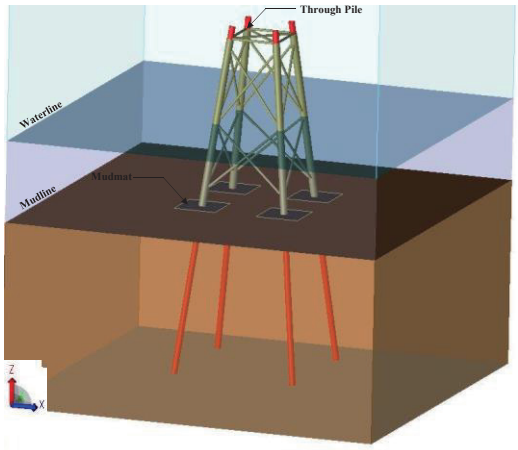

Fig. 2. Post Pile option (Through-Pile)

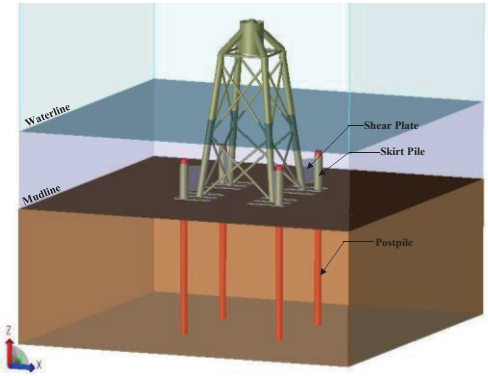

Fig. 3. Post Pile option (Skirt Pile)

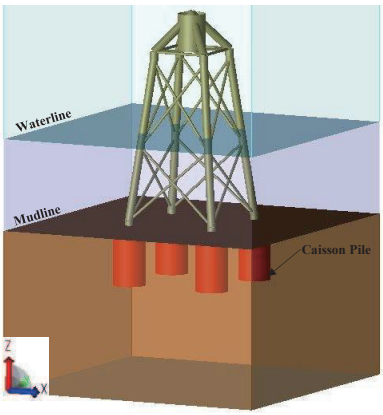

Fig. 4. Pile Caisson option

Even though the prepiled jacket is the most preferred option, only a few harvesters installed this pin-pile (prepile) jacket in active seismic zones (Changhua OWF in Taiwan). Moreover, a limited experimental study has been carried out on these prepiled jackets to understand the foundation response under seismic loading. In this research, a jacket-equivalent wind tower model was developed and tested in a centrifuge at 60g with piles passing through the two-layered sandy soil.

3 CENTRIFUGE MODEL

3.1 Model Concept

A simplified approach was used in order to assemble the centrifuge model. Accordingly, the full-scale jacket structure was modelled using DNV software (DNV - SESAM, 2020) and performed an eigenvalue analysis to get its natural frequency. Then, the centrifuge model was designed by adjusting its mass and flexural stiffness to match the full-scale structure's dynamic properties. The turbine and tower mass used was the equivalent of a 9MW turbine.

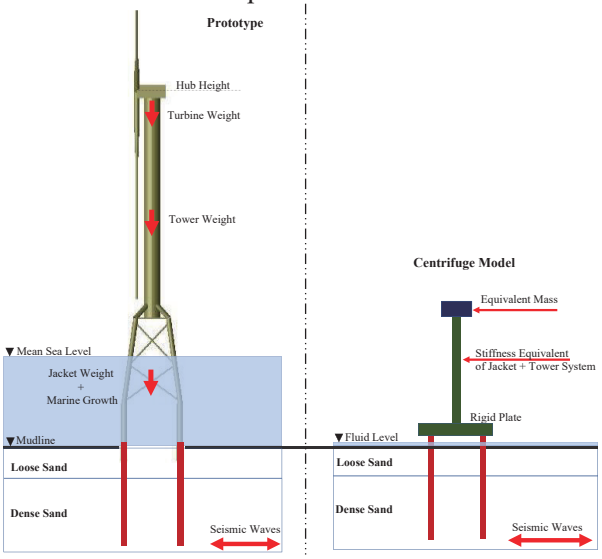

Fig. 5. Centrifuge Model

In other words, the centrifuge model's dynamic response was tuned using the full-scale jacket structure's stiffness and natural frequency. This approach also reduces the time in assembling the model for centrifuge testing. Also, it should be noted that the assembled model for centrifuge testing is the dynamic representation of the full-scale jacket and not the exact prototype.

3.2 Prototype Model design

The industry standard prepile jacket model used for eigenvalue analysis is shown in Fig 1. The parameters used for this analysis are provided in Table 1. All masses, including the entrapped water, hydrodynamic parameters and marine growth, are calculated and applied precisely for this analysis.

Table 1. Prototype Details for Eigen Analysis

Parameters	Descriptions
Water depth	20 m
Turbine Weight	475 MT
Tower Weight	325 MT
Tower Height	90 m from hub-height
Jacket Weight	700 MT
Hydrodynamic Coefficient	10% increase for anodes
For Smooth members	Cd=0.65; Cm=1.6
For Rough members	Cd=1.05; Cm=1.2
Marine Growth	100 mm full depth
Flooding	Only Jacket Legs
Others	Modified Cd & Cm for boat access ladders in Splash zone.
Boundary Condition	Fixed at the base to maximize the frequency for centrifuge model

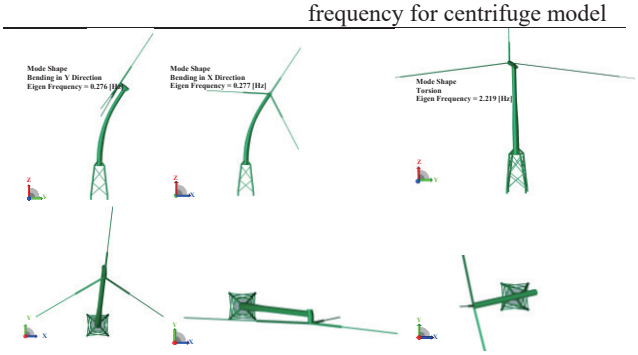

Fig. 6. Prototype Eigen Analysis (Exaggerated Mode Shape)

Based on the mass and stiffness of the prototype structure used for this analysis, the structure's first mode natural frequency is found to be 0.276 Hz. The mode shapes are shown in fig. 5. As expected, the first two-mode shapes bend horizontally, and the third shape tends towards torsion. Therefore, the structure's natural frequency lies perfectly between the 1P and 3P blade passing frequency, which is between 0.2 Hz to 0.33 Hz. Therefore, this initial frequency from the prototype model is used to design the scaled centrifuge model.

3.3 Centrifuge model design

The centrifuge model is a mass-tower design concept-based, and the primary assumption is that the wind tower and jacket sub-structure are combined into a single structural entity in the centrifuge model. Accordingly, the steel tube is designed to match the flexural stiffness of the combined tower and jacket. Thereby matching the natural frequency of the centrifuge model to the prototype model. The natural frequency, f_n of the centrifuge model is calculated using Equation 1 (Paz, 1985).

$$f_n = \frac{1}{2\pi}\sqrt{\frac{3\ E_S\ I}{L^3\left(m\ +\ \frac{m_{st\_pipe}}{4}\right)}} \tag{1}$$

Here, m is the mass at the top of the steel tube, m_{st_pipe} is the mass at the tube itself, L is the tube length. E_s and I are the young modulus of steel and second moment of area of the steel tube, respectively.

Table 2. Centrifuge Model Details

Parameters	Descriptions
Top mass (turbine)	1.052 kg
Tower mass	0.715 kg
Tower height (to Nachele)	0.75 m
Base plate (brass) connecting piles	2.6 kg
Density of steel (tower)	7.85 t/m3
Density of brass (turbine, base plate)	8.73 t/m3
Natural frequency (1st mode)	0.271 Hz
Peak dynamic overturning moment at seabed level	187 Nm
Top mass diameter (turbine)	57.08 mm
Top mass width (turbine)	52.02 mm
Base plate thickness	13.2 mm
Pile diameter (4 Nos)	22 mm

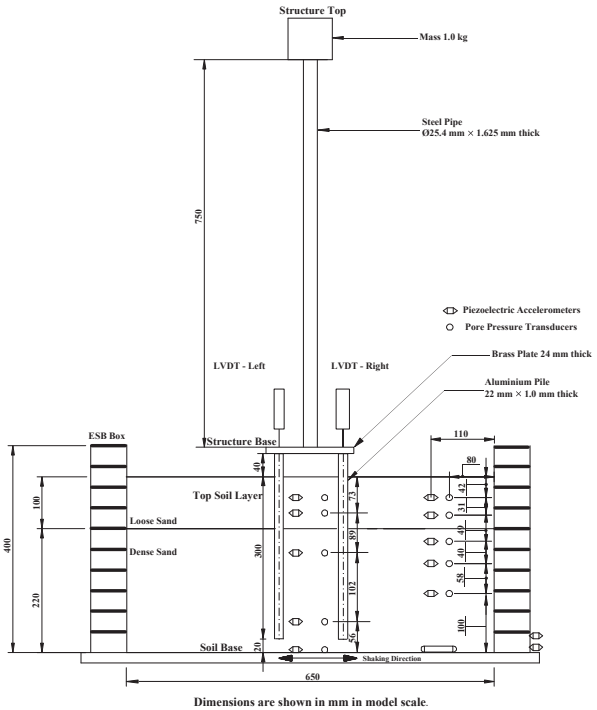

Fig. 7. Centrifuge Model with Instruments in ESB box

© 2022 KOREAN GEOTECHNICAL SOCIETY (KGS), Seoul, Korea, ISBN 978-89-952197-7-5

The peak dynamic overturning moment calculation shown in Table 2 is based on the assumed spectral acceleration of Sa = 0.3g for the initial design.

3.4 Model Test Arrangements

The experiments were conducted at 60g using the Turner beam centrifuge facility at the Schofield Centre, University of Cambridge. Hence, all centrifuge model dimensions in Fig. 6 can be converted to equivalent prototype scale using centrifuge scaling law following (Schofield, 1980) and (Madabhushi, 2014). These laws are applicable to relate the parameters in Table 2 to the prototype. Accordingly, the centrifuge model's natural frequency is 0.271 Hz, which matches the natural frequency of the prototype jacket.

Based on this model design, two centrifuge experiments were conducted (KN01-Dry test and KN02-Saturated test) and compared, first with completely dry sand to act as a benchmark and another test with a saturated condition resembling realistic offshore conditions. For the saturation test, methylcellulose was used with a viscosity of 60 cS. The two-layered sand was used with a dense layer at the bottom and the loose layer at the top. Both layers were constructed using the F65 Hoston sand and poured using the automatic sand pouring machine (Madabhushi et al., 2006). Accordingly, the relative density for loose sand was maintained at about 46 % ± 3 %, and dense sand was about 85% ± 5% for both the experiments, with the dry unit weight of loose sand at 14.5 kN/m^3 ± 1% and dense sand at 16.2 kN/m^3 ± 1% respectively.

The piezoelectric accelerometers were placed at different depths in the ESB box shown in Fig 6 to measure the acceleration generated by the air hammer device (Ghosh and Madabhushi, 2002), which generates vertically propagating shear waves in soil. In addition, the pore pressure transducers were placed beside accelerometers to measure the excess pore pressure generated during the earthquake motions.

In order to measure tower response, Micro-Electro-Mechanical-Accelerometers (MEMS) were used glued to the tower. For tower settlements, Linearly Varying Differential Transformers (LVDT's) were used and placed along the direction of the earthquake acceleration in centrifuge testing.

The scaled Imperial valley earthquake motion of 1979 and sinusoidal motions at f_n (natural frequency of the structure) and $4f_n$ earthquakes are considered for this study, and time histories are recorded and compared between dry and saturated tests. Table 3 shows the input motion used for this experiment.

Table 3. Earthquakes Input motions (g)

Earthquakes Fired	Dry Test (g)	Saturated test (g)
Sinusoidal motion at f_n	0.01	0.01
Imperial Valley (1979)	0.04	0.01
Sinuoidal motion at $4f_n$	0.20	0.16

4 EXPERIMENTAL ANALYSIS

Shear wave velocity profile is used to compare the soil stiffness variation between the dry and saturated test conditions before firing earthquake accelerations. Accordingly, the shear modulus, G_o, is calculated using Eq. 2, which relates the shear wave velocity obtained from the dry and saturated tests, respectively. The shear wave velocity and shear modulus are plotted in Fig. 8 against the prototype scale soil depth along with the semi-empirical relationships suggested by (Hardin and Drnevich, 1972) and (Oztoprak and Bolton, 2013). The results show a slight overestimate on the dry test but agree with the saturated test.

$$G_0 = \rho V_s^2 \tag{2}$$

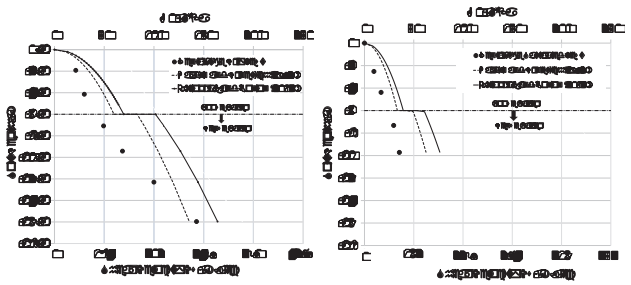

Fig. 8. Shear Velocity and Soil Stiffness Comparison

The increase in the small-strain shear modulus is consistent from loose to denser layer for both the tests. However, it is higher in the loose layer and lowers in the dense layer compared to the saturated test.

4.1 Dynamic Response of Tower

From the laboratory measurement by fixing the base of the tower, the natural frequency of the tower is measured and is found to be 0.268 Hz, which nearly matches the calculated design frequency of 0.271 Hz in the prototype scale (16.276 Hz in model scale). This confirms the model's suitability to simulate the jacket prototype.

The earthquake input motions of different intensities listed in table 3 were applied using the servo-hydraulic earthquake actuator for dry and saturated tests to compare the tower and soil response.

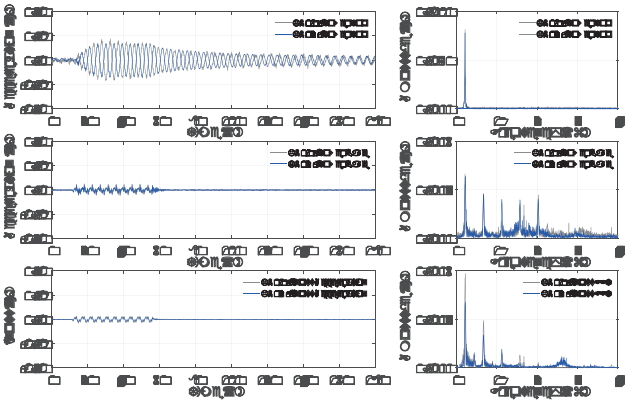

Fig. 9. Dynamic response of the tower under sinusoidal input motion correspond to natural frequency f_n

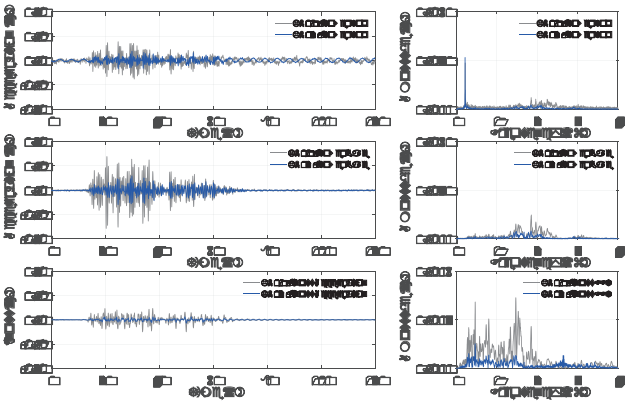

Fig. 10. Dynamic response of the tower under scaled Imperial Valley Earthquake (1979)

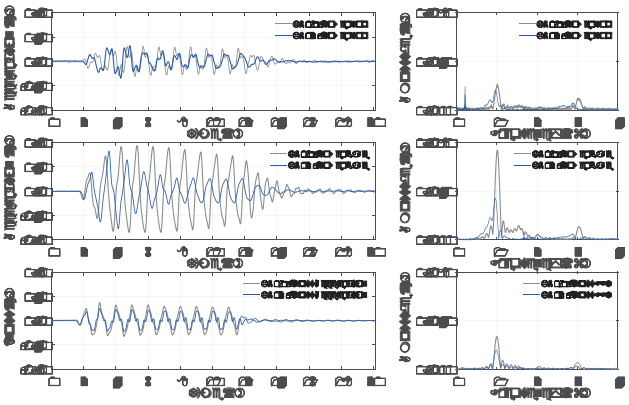

Fig. 11. Dynamic response of the tower under sinusoidal input motion correspond to natural frequency $4f_n$

The acceleration time histories and corresponding fast Fourier transforms (FFT) were plotted by processing the acquired data as shown in Figs. 9 to 11. Also, the earthquake response from tower top, tower base, and respective input motions from both tests were overlapped for comparison.

In Fig. 9, a small-amplitude earthquake motion corresponding to the natural frequency f_n of the structure is fired to ascertain the response of the structure. It is evident that the structure's response is very high, and apparent sinusoidal motion for both the tests and the FFT shown on the right side indicates the tower frequency of 0.22 Hz. This frequency is well within the recommended range for a 9MW turbine, between the 1P and 3P cut-in speeds. Also, the structure's frequency is lower than the calculated frequency of 0.271 Hz. This is due to the soil-structure interaction effects in the centrifuge model compared to the fixed base. While the input motion is only 0.01g, the structure's response at the base and top is 0.02g and 0.09g, respectively. The response is very similar for both the tests.

In Fig 10, the scaled Imperial valley earthquake motions were plotted to understand the tower response under realistic earthquake motions. While the tower base structure responds to this frequency, a minimal response from the tower top was observed except for 0.22 Hz, which shows high amplification due to resonant vibrations of the tower.

In Fig 11, the input acceleration with ten cycle excitation at four times the structure's natural frequency ($4f_n$) was considered. While the entire structure responds to this strong input motion, the tower top responded to both input frequency (0.8 Hz) as well as its natural frequency (0.22 Hz), and the tower base responded only to the input frequency. Also, at the tower base, the dry test shows a higher response continuously for the nearly first eight cycles with very low damping than in the saturated test, where the amplitude reduces with an increasing number of cycles.

4.2 Dynamic Response of Soil

The soil response is very similar in the low-intensity earthquake accelerations for dry and saturated tests. In fig. 12, the input response is marginally attenuated, while the response at other soil depths is similar. Also, the loose soil layer shows a slightly higher response than the dense layer but is not significant.

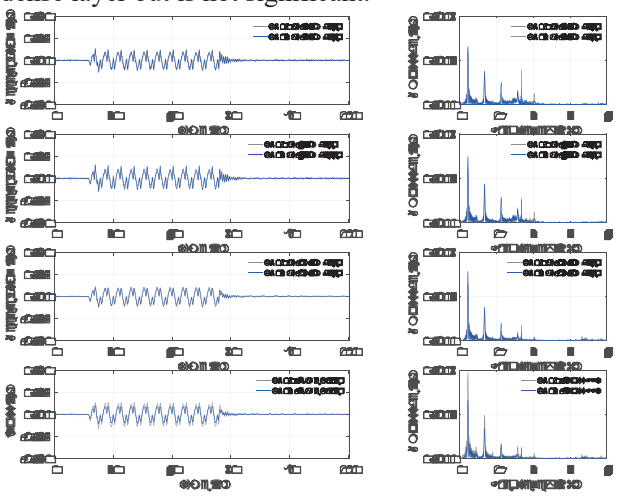

Fig. 12. Dynamic response of the soil at natural frequency f_n of the structure

However, when the earthquake intensity increases, the saturated test's soil response shows significant attenuation at all the soil depths. Fig. 13 clearly shows the stronger response for the dry test than the saturated test. This is clearly due to the transmissibility of shear waves and damping in the soil in dry soil (Rollins et al., 1998).

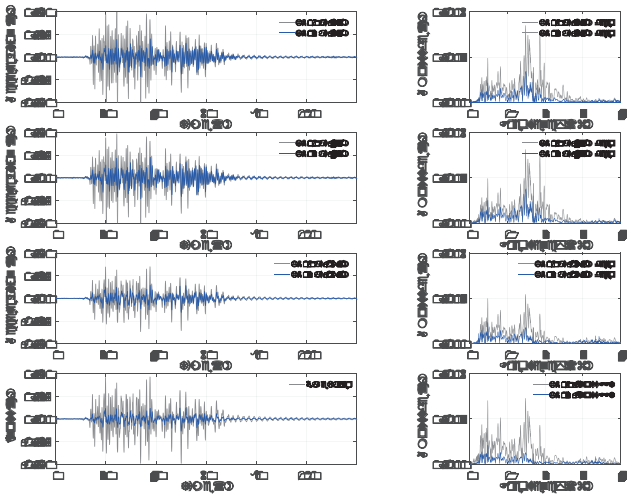

Fig. 14. Dynamic response of the soil under scaled Imperial Valley Earthquake (1979)

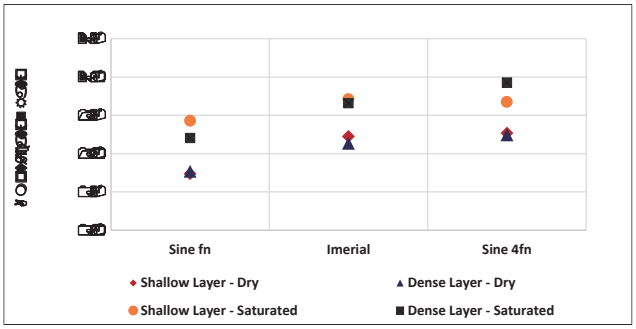

Fig. 15. Amplification Ratio

The amplification ratio calculated as a ratio of peak acceleration at the soil surface to the peak input acceleration, shown in fig. 15, increase when the intensity of the earthquake acceleration increases. Also, there is not much difference between dense and loose sand layers in the dry test. The loose layer shows some amplification in the saturated test at low-intensity earthquakes, but when the soil starts to liquefy at a higher magnitude, the dense layer shows a stronger response.

5 SETTLEMENT AND ROTATION

The settlement and rotation of the OWT occur due to soil liquefaction. It is observed from Fig 16 that in the saturated test, the structure undergoes a significant settlement of nearly 400mm and a tilt of 0.55 deg. The residual settlement and rotation are quite small in the dry test, although the transient peaks are significant. Also, the structure shows very little response to other earthquakes. As per DNV (DNVGL-ST-0126, 2018), the tilt observed in the saturated test exceeds the maximum allowable limit of 0.5. However, this limit is restricted only to monopiles, and no codal guidance is provided for the jacket structures.

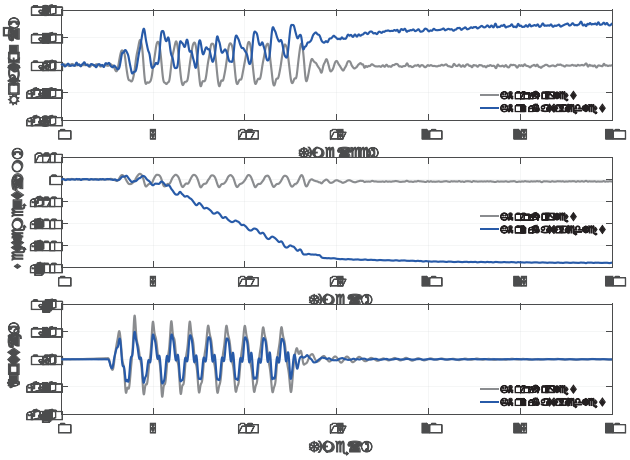

Fig. 16. Settlement under sinusoidal input motion correspond to natural frequency $4f_n$

In the saturated test, the structure was placed 2.5m (prototype scale) above the ground, but in offshore, this stick-up height is usually between 2.5 and 5m for a prepiled solution. This leads the structure more prone to larger settlements. Further studies and tests are in progress to understand the structure and soil response under stronger earthquakes by applying more realistic offshore wind turbine operational wind/wave loads in conjunction with seismic loading.

6 CONCLUSION

The dynamic response of the structure and soils shows a marginal difference between dry and saturated tests under low-intensity small-amplitude earthquakes. However, stronger earthquake shows significant amplification in the dry test and severe attenuation in a saturated condition. The structure shows a minimal post-earthquake settlement in the dry test. The effect of soil liquefaction is crucial in considering the pile foundation settlement. Hence, between the two tests, the dry test may still be considered a reference, to which other tests may be referred, but a saturated test is paramount to consider the appropriate and realistic response from offshore wind farm structures.

The main findings of this research thus far are that under stronger earthquakes, soil not only liquefies the loose top layer but also reduces the stiffness of the dense layer at a depth of 16m below the soil surface, ultimately reducing the pile shaft capacity, which tends to increase pile settlement.

Also, the settlement due to the excessive soil liquefaction is significantly higher than the usual

serviceability limit without applying operational wind loads. More tests are underway, including realistic offshore wind turbines loads to access the scale of serviceability limit exceedance. There are no precise limits in any codal provisions available for jacket rotation or settlement criteria. Hence, this extended research work may provide information to standardize the jacket design criteria for the SLS limit state.

ACKNOWLEDGEMENTS

The authors would like to express their gratitude to the technicians at the Schofield Centre of Cambridge University for their assistance during the centrifuge experiments.

REFERENCES

DNV - SESAM, 2020. Genie V7.14 - Structural Analysis Software.

DNVGL-ST-0126, 2018. Support structures for wind turbines.DNVGL.

Ghosh, B., Madabhushi, S.P.G., 2002. An efficient tool for measuring shear wave velocity in the centrifuge. International Conference on Physical Modelling in Geotechnics 119–124.

Hao, Y., Zeng, X., Wang, X., 2013. Seismic centrifuge modelling of offshore wind turbine with tripod foundation, in 2013 IEEE Energytech. IEEE, Cleveland, OH, USA, pp. 1–5. https://doi.org/10.1109/EnergyTech.2013.6645350

Hardin, B.O., Drnevich, V.P., 1972. Shear Modulus and Damping in Soils: Design Equations and Curves. J. Soil Mech. and Found. Div. 98, 667–692. https://doi.org/10.1061/JSFEAQ.0001760

Madabhushi, S.P.G., 2014. Centrifuge Modelling for Civil Engineers. CRC Press, Taylor & Francis Group, LLC.

Madabhushi, S.P.G., Houghton, N.E., Haigh, S.K. (Eds.), 2006. A new automatic sand pourer for model preparation at the University of Cambridge. Physical Modelling in Geotechnics. https://doi.org/10.1201/NOE0415415866

Oztoprak, S., Bolton, M.D., 2013. Stiffness of sands through a laboratory test database. Géotechnique 63, 54–70. https://doi.org/10.1680/geot.10.P.078

Paz, M., 1985. Structural Dynamics Theory and Computation, Third. ed. Van Nostrand Reinhold.

Rollins, K., Evans, M.D., Diehl, N.B., William, D., 1998. Shear Modulus and Damping Relationships for Gravels. Journal of Geotechnical and Geoenvironmental Engineering 124, 396–405. https://doi.org/10.1061/(ASCE)1090-0241(1998)124:5(396)

Schofield, A.N., 1980. Cambridge Geotechnical Centrifuge Operations. Géotechnique 30, 227–268. https://doi.org/10.1680/geot.1980.30.3.227